Research Article | Vol. 32, No. 7 / 25 Mar 2024 / Optics Express 11182
Optics EXPRESS

Energetic picosecond 10.2-μm pulses generated in a BGGSe crystal for nonlinear seeding of terawatt-class CO_2 amplifiers

YA-PO YANG,[1,2,*] JHENG-YU LEE,[1,2] AND JYHPYNG WANG[2,3]

[1]Molecular Science and Technology, Taiwan International Graduate Program, Academia Sinica, National Central University, Taiwan
[2]Department of Physics, National Central University, Zhongli 320317, Taiwan
[3]Institute of Atomic and Molecular Sciences, Academia Sinica, Taipei 106319, Taiwan
*albert7015@gmail.com

Abstract: We demonstrate what we believe to be a new approach to energetic picosecond 10.2-μm pulse generation based on nonlinear mixing of subnanosecond single-frequency 1338-nm pulses and broadband 1540-nm chirped pulses in a BGGSe crystal followed by a grating compressor for the purpose of seeding high-power CO_2 amplifiers. The energy of the 10.2-μm pulses exceeding 60 μJ with 3.4%-rms fluctuation can be routinely obtained. Single-shot pulse duration measurement, performed by Kerr polarization rotation time-resolved by a streak camera, together with the pulse spectrum, indicates the pulse width is between 2.7-3 ps. Numerical calculations show that power broadening and dynamic gain saturation with Rabi-flopping can be induced with such an intense seed in a multi-atmospheric CO_2 amplifier. These nonlinear effects greatly suppresses pulse splitting due to the comb-like spectrum of the CO_2 molecule. A peak power exceeding 1 TW is expected after multipass of amplification while maintaining an appropriate high intensity by controlling the beam size along the path.

1. Introduction

High-energy short-pulse lasers in the long-wavelength infrared (LWIR) regime of 8-15 μm are useful for molecular spectroscopy [1], hyperspectral imaging [2], high-harmonic generation in solid [3], strong-field science [4], and seeding for high-power CO_2 amplifier system [5,6]. Terawatt-class LWIR pulses, which have been produced from either natural or isotopic CO_2 lasers [7,8], are of great interest for laser-driven ion acceleration [9,10], inertial confinement fusion [11], laser wakefield acceleration [12], and mega-filament generation in the atmosphere [13]. The comb-like rotational-vibrational spectrum of the CO_2 molecule results in pulse splitting [8]. Pressure broadening in high-pressure CO_2 amplifier can mitigate the pulse splitting problem; however, the required gas pressure of >10 bar reaches the practical limit for producing a uniform gas discharge. Optically pumped high-pressure CO_2 amplifier by a Fe:ZnSe laser offers a smooth spectrum and THz bandwidth without the gas discharge problem, but the limited energy of Fe:ZnSe laser restricts the output energy of the CO_2 amplifier to the 1-mJ level [14]. Alternatively, isotopic CO_2 gas mixture adds shifted rotational-vibrational spectral lines between the rotational lines of the natural CO_2 molecule [15]. With a multi-bar isotopic gas mixture, an isotopic CO_2 amplifier smoothens the gain spectrum and makes it more suitable for chirped-pulse amplification [8]. Power broadening (AC Stark effect) through high-intensity seeding together with pressure broadening has been proved to be an inexpensive method to smooth out the comb-like spectrum and produce more than a Joule of energy [7]. With this method, an intensity of 5 GW/cm^2 in a 1-bar amplifier has a broadening effect comparable to a 10-bar amplifier [7]. Pulse splitting cannot be fully overcome by power broadening because the effect is weak at the low-intensity pedestal of the seed pulse. An energy ratio of 45% in the leading pulse has been reported [7].

#517743 https://doi.org/10.1364/OE.517743
Journal © 2024 Received 23 Jan 2024; revised 29 Feb 2024; accepted 29 Feb 2024; published 12 Mar 2024

Optics EXPRESS

Nevertheless, in typical laser-plasma experiments, the post pulses arriving tens of ps after the leading pulse are too late to affect the experiments. In comparison to the 10P branch of the CO_2 rotational-vibrational spectrum, the 10R branch has a ~1.6 times denser rotational lines. Although the bandwidth of the 10R branch is ~1.3 times narrower than that of the 10P branch, it still has enough bandwidth for amplifying few-picosecond pulses [15]. For the natural CO_2 molecule, the emission cross-section of the 10R branch is ~1.15 times larger than that of the 9R branch. Whereas for the isotopic CO_2 molecule that ratio is reversed [8]. Because a >50-μJ few-picosecond LWIR seed is not available, high-intensity seeding of a large-aperture multi-bar CO_2 amplifier, which mainly relies on power broadening to suppress pulse splitting, has not been achieved yet.

Several schemes to produce LWIR pulses promising for seeding a CO_2 amplifier have been developed, including difference frequency generation (DFG) of solid-state lasers [5,16] and DFG of Raman-shifted pulses [17]. Solid-state DFG has the advantages of high stability and compactness. Additionally, the signal pulse can be generated from the pump laser via either a Raman shifter [18] or supercontinuum generation [19]. Sub-ps DFG has achieved widely tunable and up to 25-μJ pulses at 10 μm with an energy fluctuation of ~30% [20]; however, laser-induced damage limits the pulse fluence and hence the achievable energy for typical aperture size of nonlinear crystals. DFG pumped with sub-ns pulses and seeded with sub-ns chirped pulses has advantages in electronic synchronization of the pump and signal lasers [21], increasing pump fluence, and reducing nonlinear absorptions, except that a longer nonlinear crystal should be used as the intensity of the mixing pulses is reduced. It also solves the problem of temporal walk-off due to group-delay mismatch in sub-ps DFG. Several DFG approaches based on non-oxide nonlinear crystals have been presented in the literature [22]. To avoid either one-photon or two-photon absorption in the nonlinear crystals, many approaches implement two-stage schemes where near-IR (NIR) pulses, typically from a Ti:sapphire laser, are firstly down-converted to short-wavelength infrared pulses and then down-converted to LWIR pulses. To circumvent the linear and nonlinear absorption problems in a nonlinear crystal, we found that the convenient lasing transitions of Nd:YAG at 1319 nm and 1338 nm can be utilized to mix with 1540-nm chirped pulses produced from an Er:fiber laser followed by a stretcher, in a nonlinear crystal to generate 9.2-μm/10.2-μm chirped pulses. The generated LWIR pulses can gain energy in a CO_2 amplifier as their spectra coincide with the 9R/10R branch of the CO_2 molecule. Therefore, a compact single-stage DFG based on a 1.3-μm Nd:YAG laser and a 1540-nm Er:fiber laser with a chirped signal pulse can be realized.

For nonlinear wave mixing in the LWIR regime, GaSe crystal is a common choice because of its high nonlinearity (d_{22} ~ 54 pm/V) with a wide transparency range of 0.65-18 μm [23] and availability; however, it is fragile and difficult to be coated or cut in desired orientation due to its mica-like crystal structure. BGGSe ($BaGa_2GeSe_6$) crystal is a neoteric nonlinear crystal which also features high nonlinearity (d_{eff} ~ 35 pm/V at our setup) with a wide transparency range (0.6-18 μm) [24,25]. In addition, it has a two-photon absorption edge at ~1.1-μm due to its bandgap of ~2.3 eV [25] and high optical damage threshold of ~2.3 J/cm^2 (7.6 ns, 1053 nm, 100 Hz) [26]. Owing to its good mechanical properties, cutting in selected orientation and antireflection coating are possible [27]. Moreover, it is nonhygroscopic and chemically stable, showing no surface aging effect [27]. Large BGGSe boules of ϕ40 mm × 100 mm have been grown by the vertical Bridgman–Stockbarger method with high optical quality [25,28]. These superior properties make BGGSe a promising nonlinear material for producing energetic LWIR pulses by DFG [28].

In this paper, we demonstrate a new approach based on DFG with a chirped signal pulse in a BGGSe nonlinear crystal to generate 60-μJ few-picosecond 10.2-μm pulses (Sec. 2.). An electronically synchronized 1338-nm pulse from a seeded regenerative amplifier is mixed with an amplified 1540-nm chirped pulse in the BGGSe crystal. The NIR pulses produced from

Optics EXPRESS

solid-state lasers and amplifiers (Sec. 3.) yield a stable (~3.4% fluctuation) and low drift (~0.5%/hr) 10.2-μm pulse. To measure the pulse duration of the generated 10.2-μm pulse, we construct a single-shot pulse duration measurement system based on Kerr polarization rotation of a 669-nm probe pulse induced by the 10.2-um pulse (Sec. 4.). The polarization-rotated probe pulse is measured by a streak camera with a 2-ps resolution and a >200 ps range. We also numerically calculate the pulse evolutions in a 40-cm 4-bar CO_2 amplifier when seeded with the intense 10.2-μm pulse (Sec. 5.). By properly managing the intensity with focusing mirrors and diffraction, power broadening and dynamic gain saturation with Rabi-flopping can be maintained along the beam path in the CO_2 amplifier. A peak power exceeding 1 TW and ~50% of energy contained in the leading pulse are expected after five passes of amplification.

2. Generation of energetic picosecond 10.2-μm pulses

Figure 1 shows the schematic diagram of our experimental setup. A 1.5-μm femtosecond pulse train with 50-MHz repetition rate is generated from an Er:fiber oscillator (ITRI, Taiwan). A chirped-fiber Bragg grating (TeraXion, Canada) stretches the 1.5-μm pulse to ~500 ps with a group-delay dispersion (GDD) of -81.7 ps^2 and extracts a bandwidth of ~8 nm at 1540 nm. The 1540-nm chirped pulse of ~0.5 nJ is amplfied to ~200 μJ by a laser-pumped optical parametric chirped-pulse amplifier (OPCPA) based on a 15-mm long 5 mol.% MgO doped periodic-poled lithium niobate (PPLN, type-0 (e=e-e), Λ = 30.35 μm, phase-matching temperature ~ 62°C. HC photonics, Taiwan). The pump laser is a seeded regenerative amplifier of 1064 nm with 600-ps and 8-mJ of energy. A single-pass gain of ~400,000 can be obtained with this amplifier when pumped with an intensity of ~2 GW/cm^2.

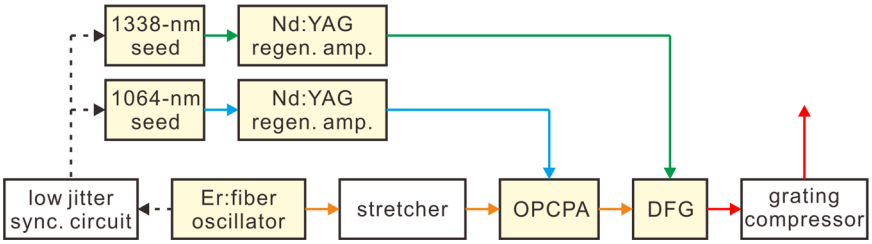

Fig. 1. Schematic diagram of the 10.2-μm generator system taking a space of only 90 cm × 90 cm.

Due to the gain narrowing effect resulted from the phase-matching bandwidth and the intensity dependent gain of the OPCPA, the spectral width of the amplified 1540-nm pulse is reduced to ~1.6 nm. Figure 2 shows the energy stability of the amplified 1540-nm pulse. Short-term fluctuation of ~1.4%-rms and long-term drift of ~0.2%/hr are achieved with crystal temperature fluctuation <10 mK and the pump laser fluctuation <1%-rms. The phase-matching condition of the PPLN OPCPA depends on crystal temperature due to temperature-dependent refractive indices. As the gain profile shifts with a coefficient of ~0.28 nm/K, the peak gain varies ~0.3% per K or ~17% per 10 K.

Positively chirped 10.2-μm pulses are generated by the DFG process when mixing the 1338-nm pulses and the negatively chirped 1540-nm pulses in a 10-mm long BGGSe crystal (type-II (o=o-e), θ = 27.3°, ϕ = 12.7°. DIEN TECH, China). The temporal and spatial walk-off are ~1.5 ps and ~250 μm. Chirp reversal of the generated 10.2-μm pulse results from down-conversion of the 1540-nm chirped pulse by a single-frequency 1338-nm pulse [29]. Pumped by a 4.3-mJ 380-ps 1338-nm pulse at a peak intensity of ~1.3 GW/cm^2, the 1540-nm chirped pulse is amplified from ~200 μJ to ~1 mJ. Meanwhile, a 10.2-μm chirped pulse with ~120-μJ energy

Optics EXPRESS

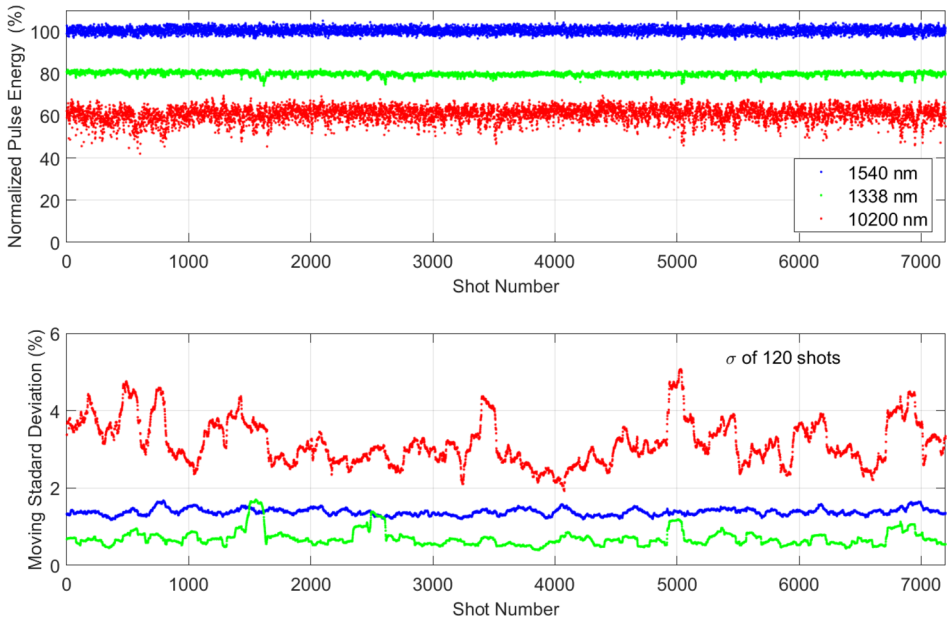

Fig. 2. Energy stabilities and 120-shot moving standard deviation of the 1338-nm pulses (green), the 1540-nm pulses (blue), and the compressed 10.2-μm pulses (red).

is also generated. The output beam profiles of the 1540-nm and 10.2-μm chirped pulses are measured with a pyrocamera (PY-III-HR-C-A-PRO, Ophir) and shown in Fig. 3.

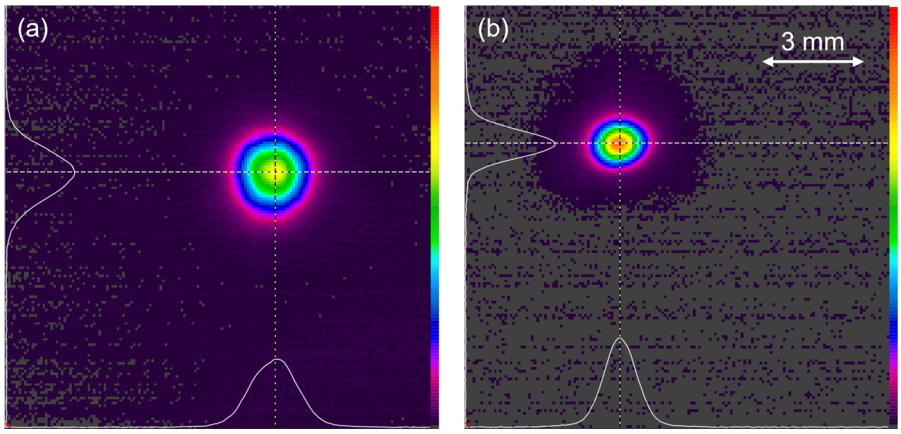

Fig. 3. The measured beam profile of (a) the ~200-μJ 1540-nm and (b) the generated 10.2-μm chirped pulses.

After compensation of the positive chirp of the 10.2-μm pulse in a Treacy-type grating compressor [30], the output energy can be up to 60 μJ. Figure 2 shows the energy stability of the compressed 10.2-μm pulse measured with a pyroelectric energy meter (J-10MB-LE, Coherent). Short-term stability of ~3.4%-rms and long-term drift of <0.5%/hr are achieved. By varying the pump energy, the DFG stage is approaching saturation as shown in Fig. 4. As an example, our approach can be scaled to produce few-picosecond 10.2-μm pulses with >1-mJ energy when a 7-mm aperture BGGSe crystal and higher energy Nd:YAG lasers are employed.

Optics EXPRESS

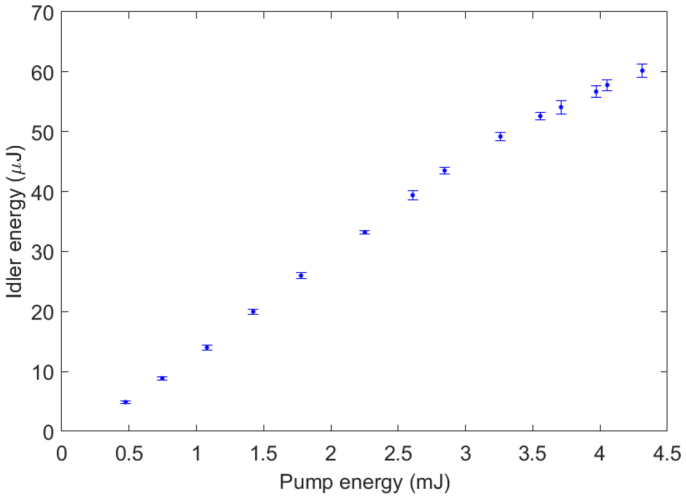

Fig. 4. The energy of the compressed 10.2-μm pulse respects to the 1338-nm pump energy.

The spectrum of the 10.2-μm pulse is measured by a polychromator with a 256-pixel pyroelectric detector array (DIAS, Germany) as shown in Fig. 5. Efficient seeding of a CO_2 amplifier can be achieved with this 10.2-μm pulse since the 10R-branch of the CO_2 molecule overlaps with the entire spectrum of the 10.2-μm pulse.

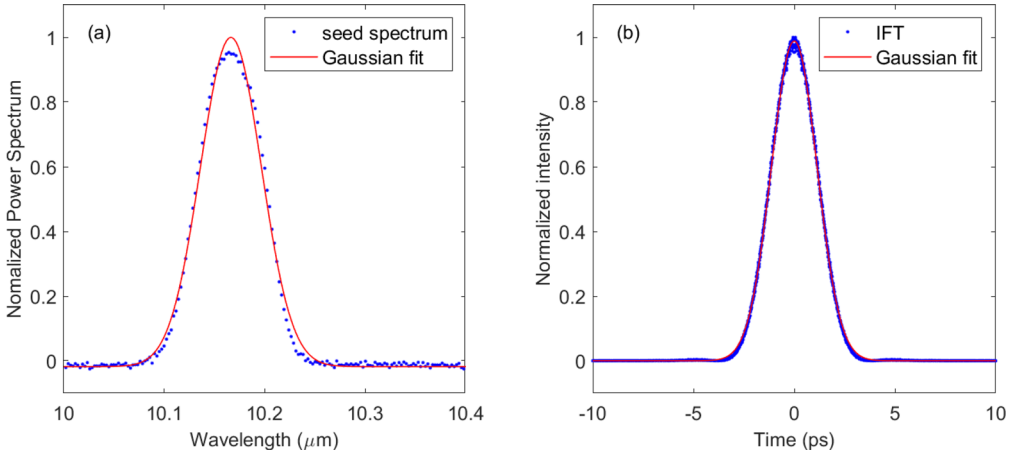

Fig. 5. (a)The measured seed spectrum and (b)its inverse-Fourier-transformed temporal profile assuming no chirp.

3. Electronically synchronized sub-ns Nd:YAG lasers

The electronically synchronized 1064-nm and 1338-nm lasers share a similar configuration, which is composed of a single-frequency continuous-wave (CW) laser, an intensity modulator, and a Nd:YAG regenerative amplifier. Both lasers run at a 2-Hz repetition rate. The 1064-nm CW laser is a commercial single-frequency laser (NP Photonics, Germany) with an output power of >30 mW. The 1338-nm CW laser is made with an external-cavity diode laser with an output power of >3 mW and wavelength tunability from 1310 nm to 1345 nm. These CW lasers are amplitude-modulated to produce hundreds of picosecond pulses with fiber-coupled Mach-Zehnder

Optics EXPRESS

intensity modulators (Optilab, USA). The modulators are driven by a pulse generator composed of emitter-coupled logic gates and a 2.5-GHz RF amplifier. The timing jitter with respect to the 1540-nm pulse is ~11 ps-rms. One of the problems when using $LiNbO_3$ Mach-Zehnder modulators is that interference conditions vary with temperature, bias electric field distribution, etc., resulting in a drifting CW background [31]. Therefore, a digital feedback loop based on lock-in detection (minimum finding from first-order derivative) [32] and proportional-integral control is adopted to maintain a minimum CW background.

Diode-pumped Nd:YAG regenerative amplifiers are constructed to boost the energy of the sub-ns seeds to the required millijoule level with an energy gain of $>10^8$. For the 1338-nm amplifier, measures have been taken to avoid parasitic lasing or amplified spontaneous emission (ASE) of the strong 1064-nm line and the nearby 1319-nm line. The cavity mirrors are high reflectance at 1.3 μm and high transmittance at 1064 nm so that parasitic lasing and ASE of 1064 nm are prevented. To avoid ASE and gain competition from the 1319-nm emission, a 2720-μm thick birefringent plate of quartz is placed in the 1338-nm amplifier at Brewster's angle. The birefringent plate acts as a high-order waveplate that effectively provides λ/2 retardence for one line and zero or λ retardence for the other line. Therefore, the cavity loss for the two 1.3-μm lines can be controlled by tilting the quartz plate to suppress the 1319-nm lasing. The 1338-nm amplifier delivers ~380-ps pulses with >6-mJ energy and <1% fluctuation. The 1064-nm amplifier delivers ~600-ps pulses with >10-mJ energy and <1% fluctuation. Output beam profiles for both amplifiers are near TEM_{00} mode as expected from a regenerative amplifier with a stable cavity.

Characterization of the temporal profile of these lasers is crucial since the CW lasers may lase at more than one longitudinal mode in some circumstances. Unstable envelope oscillation originating from multi-longitudinal mode beating will cause spectral modulation of the idler pulse through DFG and ruin the energy stability of the idler pulse. Figure 6 shows single- and multi-longitudinal mode 669-nm pulses that are frequency doubled from the 1338-nm laser and measured by a Hamamatsu streak camera.

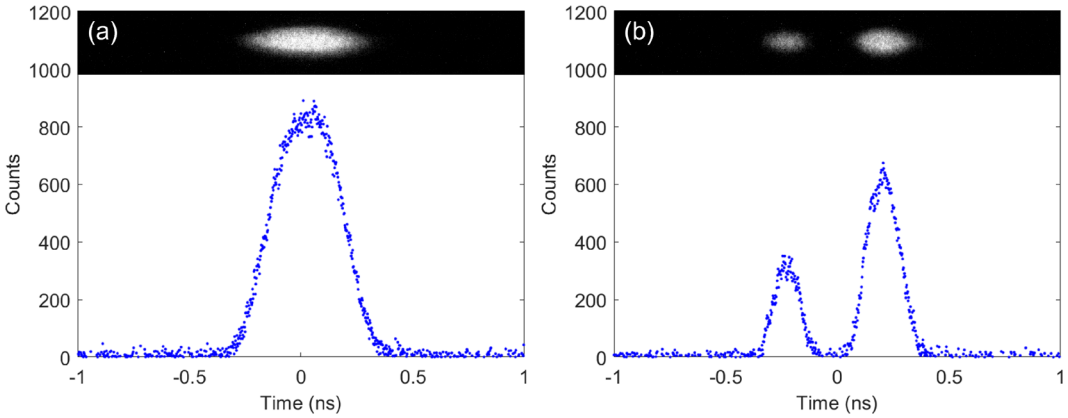

Fig. 6. The measured (a)single- and (b)multi-longitudinal mode pulses. The upper parts of the figure are the streak-camera images.

4. Single-shot pulse duration measurement of LWIR pulses

Single-shot pulse duration measurement of a microjoule-level few-picosecond pulse in the LWIR regime is non-trivial, especially when energetic sub-ps synchronized NIR pulses are not available for up-conversion. To do that, a single-shot optical pulse diagnosis system based on Kerr polarization rotation and a streak camera is constructed. A 669-nm 280-ps pulse, prepared by

Optics EXPRESS

doubling the 1338-nm pulse, with a peak power of >10 kW is utilized as a probe to measure the change of refractive index induced by the compressed 10.2-μm pulse (pump pulse) in a 3-mm thick ZnS window via optical Kerr effect. As the probe pulse is polarized at 45° to the polarization plane of the pump pulse, the ZnS window becomes a pump-intensity-dependent phase retarder [33]. Subsequently, the polarization-rotated probe pulse passes through a crossed polarizer, and its temporal profile is measured by a streak camera. Aside from the clear benefits of single-shot measurement over scanning-based methods, this system has the capability to measure a temporal range of >200 ps with 2-ps resolution, so pulse-splitting phenomena in a CO_2 amplifier can be observed with this system as well.

Multispectral-grade ZnS polycrystalline windows have high nonlinear refractive index (n_2) of ~10^{-14} cm^2/W at 669 nm and is transparent within 0.4-12 μm [34], so it is an ideal Kerr medium for this application comparing with the toxic CS_2 liquid which has an inherent molecular relaxation time of 2 ps [35]. Another commonly used IR window material, ZnSe, also has high transparency at the probe and pump wavelengths and high n_2 of ~5×10^{-14} cm^2/W at 850 nm [34]; however, the n_2 drops to near zero at around 670 nm [34]. This is consistent with our experimental result as no nonlinear polarization effect is observed with a ZnSe polycrystalline window.

The pump and probe pulses are combined by an indium tin oxide (ITO) glass since the ITO coating possesses a carrier plasma density (carrier concentration) between the critical plasma densities of the two pulses. Consequently, the 10.2-μm pulse is reflected by the ITO coating, and the probe pulse propagates through the ITO glass. Then, the two pulses are focused at the center of the ZnS window by an f = 50 mm off-axis parabolic mirror. The estimated peak intensity of the focused 10.2-μm pulse can reach >1 GW/cm^2, which is high enough to induce a detectable change of refractive index in our setup.

The transmittance of the probe pulse is proportional to $\sin^2(n_2 I_{pp}\pi L/\lambda_{pb})$ [33], where I_{pp} is the pump intensity, L is the thickness of the Kerr medium, and λ_{pb} is the probe wavelength. A transmittance of >5% and more than 0.5 nJ transmitted energy is expected with our setup. Kerr polarization rotation is inherently free from phase mismatch as it is a degenerate four-wave mixing process, but material dispersion causes pulse broadening and thus limits the thickness of the Kerr medium.

The measured temporal profile of the transmitted probe pulse is shown in Fig. 7. As the probe pulse width τ_{pb} is close to the 2-ps temporal resolution of the streak camera, we model the temporal resolution as a 2-ps Gaussian function to be convoluted with the original probe pulse. For a Gaussian probe pulse deconvolution yields $\tau_{pb} = \sqrt{{\tau_m}^2 - (2\ \mathrm{ps})^2}$, where τ_m is the measured pulse width. The transfer function of Kerr polarization rotation of $\sin^2 I_{pp}$ is approximated as I_{pp}^2 in the small-signal regime. Therefore, the deconvoluted probe pulse duration must be multiplied by $\sqrt{2}$ to correct for the intensity-square dependence in retrieving the pump pulse duration. The retrieved pulse duration of the compressed 10.2-μm pulse is ~3 ps (FWHM), even though the bandwidth-limited duration of the 10.2-μm pulse corresponds to ~2.7 ps indicated from the inverse Fourier transformation of the measured pulse spectrum as shown in Fig. 5. This range of uncertainty is due to the limited signal-to-noise ratio and the residual high-order chirp not compensated by the compressor. The actual pulse duration should be between 2.7-3 ps.

Optics EXPRESS

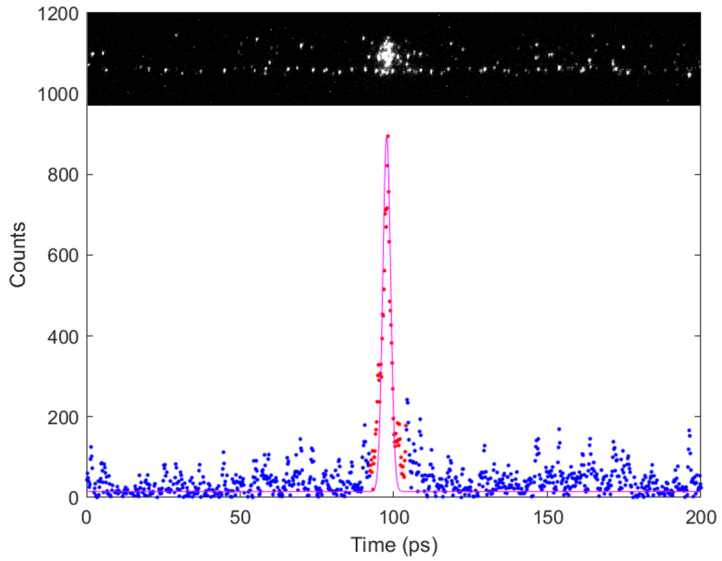

Fig. 7. Measured temporal profile of the polarization-rotated 669-nm probe. The measured width, the retrieved probe width, and the retrieved pump width are ~3 ps, ~2.2 ps, ~3 ps, respectively. Dots are data points, red dots are data points for Gaussian fit, the magenta line is the fitted line. The upper part of the figure is the streak-camera image.

5. Calculation of pulse evolution in a CO_2 amplifier

Pulse-splitting phenomena, caused by the ~35-GHz modulation [15] of the chosen 10R-branch gain spectrum, is inevitable in the entering path of a CO_2 amplifier because a seed intensity that is high enough to induce significant power broadening only appears near the focal point when the seed is focused. As the seed gains more and more energy during amplification, the broadening effect is increased and pulse splitting is reduced. To model the pulse evolution in a CO_2 amplifier, numerical solutions of the optical Bloch equations are obtained by using the fourth-order Runge-Kutta algorithm. Such a code is capable of coherent stimulation of many emission lines of the CO_2 molecule with a broadband seed [36].

Figure 8 shows the schematic diagram of the proposed 40-cm 4-bar CO_2 amplifier. The calculated evolution of the temporal profile at the center of the beam is shown in Fig. 9. The gas mixture composition is assumed to be CO_2:N_2:He = 4:1:12. In the first three passes, it is critical to focus the seed in the amplifier as power broadening near the focal point helps to prevent severe pulse splitting arising from the comb-like rotational-vibrational gain spectrum. Even though the split second pulse reaches an intensity comparable to the first pulse at the 2nd pass, its suppression starts at the 3rd pass. This is due to dynamic gain saturation as the fluence of the first pulse exceeds the saturation fluence of ~300 mJ/cm^2 under a calculated small-signal gain of ~5.7%/cm and a total population inversion density of ~10^{18}/cm^3. Pulse shortening also indicates that Rabi flopping of the lasing transition and power broadening occur [7]. The first pulse depletes most of the upper-state population with its pulse tail reabsorbed back to the upper state after half of the Rabi period. The power-broadened gain spectrum supports the required bandwidth of the shortened pulse. During the last two passes, the peak intensity of the first pulse is intentionally kept at around 400 GW/cm^2 to maintain the temporal profile while retaining 50% of the energy in the first pulse. A higher intensity can further shorten the duration of the first pulse and reduce the following side-pulses; however, this may not be practical as optical damage

Optics EXPRESS

to NaCl windows limits the highest fluence to 0.5 J/cm^2 [37]. After the 5-pass CO_2 amplifier, a 2-ps 10.2-μm pulse with a peak power exceeding 1 TW is expected.

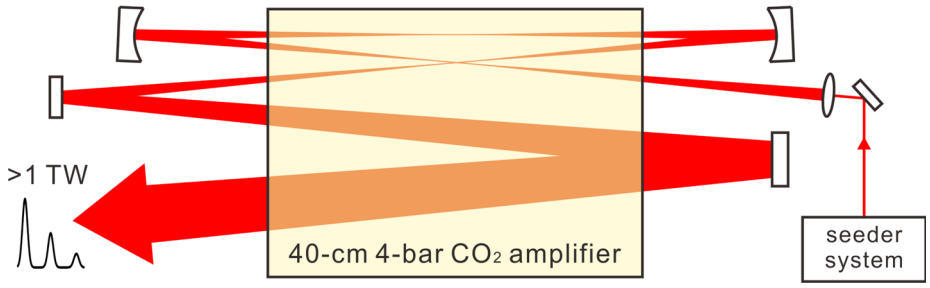

Fig. 8. Schematic diagram of the proposed 5-pass CO_2 amplifier seeded by the energetic 10.2-μm pulses.

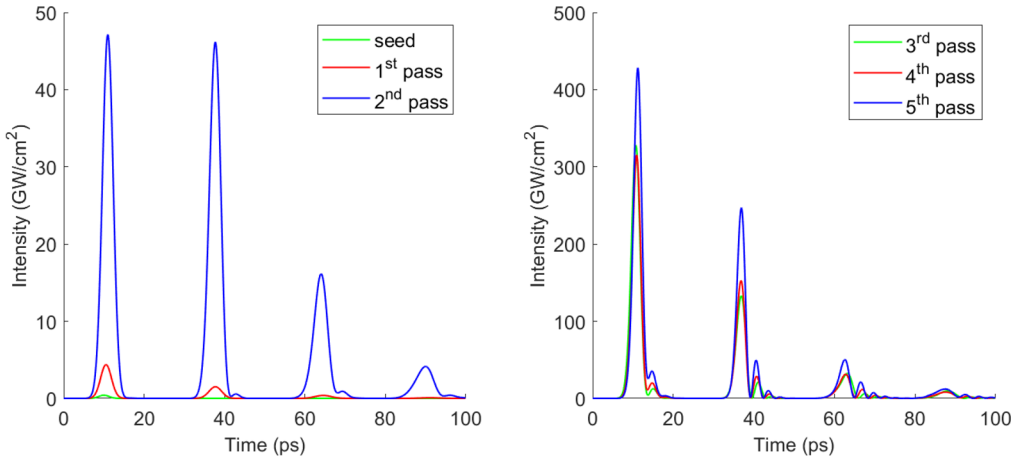

Fig. 9. Temporal intensity profiles of each pass at the output of the CO_2 amplifier.

6. Conclusion

We demonstrated an energetic few-picosecond 10.2-μm pulse generator for seeding a terawatt-level CO_2 amplifier and also characterized the performance of the seeder with thorough measurements. Our approach features DFG with a chirped signal pulse in a BGGSe nonlinear crystal, high stability and compactness, and electronic synchronization with the NIR lasers. Numerical calculations show that pulse splitting due to the comb-like gain spectrum of the CO_2 amplifier can be mitigated by nonlinear effect rather than using expensive isotopic gases. We expect a high-performance terawatt CO_2 laser for experiments in strong-field science and laboratory astrophysics can be built upon this robust seeder system.

Funding. National Science and Technology Council (MOST108-2112-M001-034, MOST109-2221-E001-024).

Acknowledgments. We thank Feng-Yen Su and Chi-Han Chen for their help with the construction of the 1064-nm regenerative amplifier and the digital feedback loop for the intensity modulators, respectively. We also acknowledge Wu-Cheng Chiang for his technical assistance in programming and graphics.

Disclosures. The authors declare no conflicts of interest.

Data availability. Data underlying the results presented in this paper are not publicly available at this time but may be obtained from the authors upon reasonable request.

Optics EXPRESS

References

1. A. S. Kowligy, H. Timmers, A. J. Lind, *et al.*, "Infrared electric field sampled frequency comb spectroscopy," Sci. Adv. **5**(6), eaaw8794 (2019).
2. M. Hermes, R. B. Morrish, L. Huot, *et al.*, "Mid-IR hyperspectral imaging for label-free histopathology and cytology," J. Opt. **20**(2), 023002 (2018).
3. S. Ghimire, A. D. DiChiara, E. Sistrunk, *et al.*, "Observation of high-order harmonic generation in a bulk crystal," Nat. Phys. **7**(2), 138–141 (2011).
4. Z. Chang, L. Fang, V. Fedorov, *et al.*, "Intense infrared lasers for strong-field science," Adv. Opt. Photonics **14**(4), 652–782 (2022).
5. E. Welch, D. Matteo, S. Tochitsky, *et al.*, "Generating quasi-single multi-terawatt picosecond pulses in the neptune CO_2 laser system," in *2018 IEEE Advanced Accelerator Concepts Workshop (AAC)*, (IEEE, 2018), pp. 1–4.
6. M. N. Polyanskiy, I. V. Pogorelsky, M. Babzien, *et al.*, "Demonstration of a 2 ps, 5 TW peak power, long-wave infrared laser based on chirped-pulse amplification with mixed-isotope CO_2 amplifiers," OSA Continuum **3**(3), 459–472 (2020).
7. D. Haberberger, S. Tochitsky, and C. Joshi, "Fifteen terawatt picosecond CO_2 laser system," Opt. Express **18**(17), 17865–17875 (2010).
8. M. N. Polyanskiy, I. V. Pogorelsky, and V. Yakimenko, "Picosecond pulse amplification in isotopic CO_2 active medium," Opt. Express **19**(8), 7717–7725 (2011).
9. T.-C. Liu, X. Shao, C.-S. Liu, *et al.*, "Laser acceleration of protons using multi-ion plasma gaseous targets," New J. Phys. **17**(2), 023018 (2015).
10. D. Haberberger, S. Tochitsky, F. Fiuza, *et al.*, "Collisionless shocks in laser-produced plasma generate monoenergetic high-energy proton beams," Nat. Phys. **8**(1), 95–99 (2012).
11. B. Shen, X. Zhao, L. Yi, *et al.*, "Inertial confinement fusion driven by long wavelength electromagnetic pulses," High Power Laser Sci. Eng. **1**(3-4), 105–109 (2013).
12. L. Zhang, B. Shen, J. Xu, *et al.*, "High quality electron bunch generation with CO_2-laser-plasma interaction," Phys. Plasmas **22**(2), 023101 (2015).
13. S. Tochitsky, E. Welch, M. Polyanskiy, *et al.*, "Megafilament in air formed by self-guided terawatt long-wavelength infrared laser," Nat. Photonics **13**(1), 41–46 (2019).
14. D. Tovey, J. Pigeon, S. Tochitsky, *et al.*, "Lasing in 15 atm CO_2 cell optically pumped by a Fe:ZnSe laser," Opt. Express **29**(20), 31455–31464 (2021).
15. C.-C. Chou, A. Maki, S. J. Tochitsky, *et al.*, "Frequency measurements and molecular constants of CO_2 $00^0 2$-$[10^0 1, 02^0 1]_{I,II}$ sequence band transitions," J. Mol. Spectrosc. **172**(1), 233–242 (1995).
16. M. N. Polyanskiy, M. Babzien, and I. V. Pogorelsky, "Chirped-pulse amplification in a CO_2 laser," Optica **2**(8), 675–681 (2015).
17. E. Welch, S. Y. Tochitsky, J. Pigeon, *et al.*, "Long-wave infrared picosecond parametric amplifier based on raman shifter technology," Opt. Express **26**(5), 5154–5163 (2018).
18. H. M. Pask, "The design and operation of solid-state raman lasers," Prog. Quantum Electron. **27**(1), 3–56 (2003).
19. J. Swiderski, "High-power mid-infrared supercontinuum sources: Current status and future perspectives," Prog. Quantum Electron. **38**(5), 189–235 (2014).
20. I. Bayanov, R. Danielius, P. Heinz, *et al.*, "Intense subpicosecond pulses tunable between 4 μm and 20 μm generated by an all-solid-state laser system," Opt. Commun. **113**(1-3), 99–104 (1994).
21. A. Galvanauskas, A. Hariharan, D. Harter, *et al.*, "High-energy femtosecond pulse amlification in a quasi-phase-matched parametric amplifier," Opt. Lett. **23**(3), 210–212 (1998).
22. V. Petrov, "Frequency down-conversion of solid-state laser sources to the mid-infrared spectral range using non-oxide nonlinear crystals," Prog. Quantum Electron. **42**, 1–106 (2015).
23. G. Abdullaev, L. Kulevskii, A. Prokhorov, *et al.*, "GaSe, a new effective material for nonlinear optics," Soviet Journal of Experimental and Theoretical Physics Letters **16**, 90 (1972).
24. K. Kato, V. V. Badikov, L. Wang, *et al.*, "Effective nonlinearity of the new quaternary chalcogenide crystal $BaGa_2GeSe_6$," Opt. Lett. **45**(8), 2136–2139 (2020).
25. V. V. Badikov, D. V. Badikov, V. B. Laptev, *et al.*, "Crystal growth and characterization of new quaternary chalcogenide nonlinear crystals for the mid-IR: $BaGa_2GeS_6$ and $BaGa_2GeSe_6$," Opt. Mater. Express **6**(9), 2933–2938 (2016).
26. N. Y. Kostyukova, A. A. Boyko, E. Y. Erushin, *et al.*, "Laser-induced damage threshold of $BaGa_4Se_7$ and $BaGa_2GeSe_6$ nonlinear crystals at 1.053 μm," J. Opt. Soc. Am. B **36**(8), 2260–2265 (2019).
27. U. Elu, L. Maidment, L. Vamos, *et al.*, "Few-cycle mid-infrared pulses from $BaGa_2GeSe_6$," Opt. Lett. **45**(13), 3813–3815 (2020).
28. V. Petrov, V. V. Badikov, D. V. Badikov, *et al.*, "Barium nonlinear optical crystals for the mid-IR: characterization and some applications," J. Opt. Soc. Am. B **38**(8), B46–B58 (2021).
29. A. Piskarskas, A. Stabinis, and A. Yankauskas, "Phase phenomena in parametric amplifiers and generators of ultrashort light pulses," Sov. Phys. Usp. **29**(9), 869–879 (1986).
30. E. Treacy, "Optical pulse compression with diffraction gratings," IEEE J. Quantum Electron. **5**(9), 454–458 (1969).
31. J. P. Salvestrini, L. Guilbert, M. Fontana, *et al.*, "Analysis and control of the DC drift in $LiNbO_3$ based Mach–Zehnder modulators," J. Lightwave Technol. **29**(10), 1522–1534 (2011).
32. P. Horowitz and W. Hill, *The Art of Electronics* (Cambridge University Press, 2015), 3rd ed.

Optics EXPRESS

33. T. Owen, L. Coleman, and T. Burgess, "Ultrafast optical kerr effect in CS_2 at 10.6 μm," Appl. Phys. Lett. **22**(6), 272–273 (1973).
34. T. R. Ensley and N. K. Bambha, "Ultrafast nonlinear refraction measurements of infrared transmitting materials in the mid-wave infrared," Opt. Express **27**(26), 37940–37951 (2019).
35. M. Duguay and A. Mattick, "Ultrahigh speed photography of picosecond light pulses and echoes," Appl. Opt. **10**(9), 2162–2170 (1971).
36. V. T. Platonenko and V. D. Taranukhin, "Coherent amplification of light pulses in media with a discrete spectrum," Sov. J. Quantum Electron. **13**(11), 1459–1466 (1983).
37. P. Corkum, "Amplification of picosecond 10 μm pulses in multiatmosphere CO_2 lasers," IEEE J. Quantum Electron. **21**(3), 216–232 (1985).